The Effect of Aluminium Addition on Solid Solution Strengthening in CoCrFeMnNi High Entropy Alloy: Experiment and Modelling

Jitesh Kumar, N P Gurao and Krishanu Biswas[#]

Department of Material Science & Engineering, Indian Institute of Technology Kanpur -208016, India

Graphical Abstract

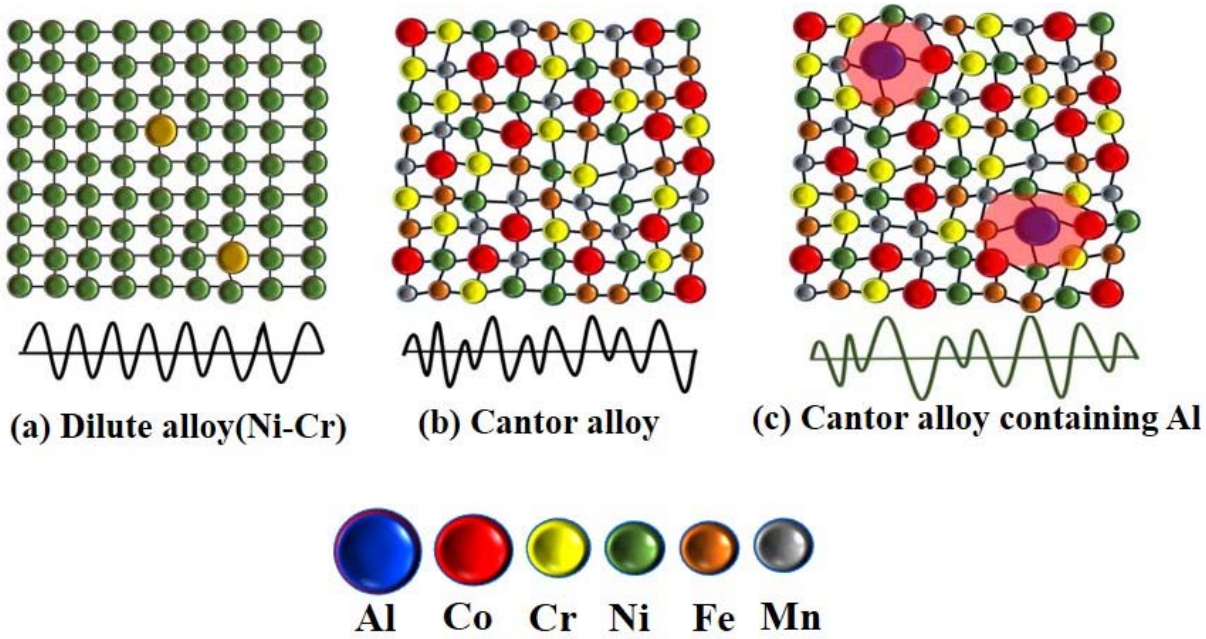

[#]Corresponding author: email: kbiswas@iitk.ac.in, Phone: +91-5126796184, FAX: +91-5126797505

Abstract

The effect of aluminium addition to the Cantor alloy in the composition regime of 0.25-5 atomic percent on solid solution strengthening of single phase HEA was investigated using experiments and constitutive modeling. The continuous increase in yield and tensile strength without significant change in ductility is observed for the alloys characterized by almost similar grain sizes (~100μm) with increasing aluminium content. The constitute modeling of the strengthening has been performed using traditional as well as recently developed models for solid solution strengthening. The constitutive modeling indicated significant contribution of solid solution strengthening due to addition of Al having relatively larger size (~12%) than the size of elements in the Cantor alloy leading to severe local lattice distortion. The experimental yield strength could be best explained on the basis of large apparent distortion volume of Al atom acting as a stronger barrier to dislocation motion based on the Varvenne model.

Keywords: High Entropy Alloys, Aluminium addition, Lattice distortion, Solid solution strengthening, Yield strength, Constitutive Modeling

1. Introduction

Achieving high strength with sufficient ductility and fracture toughness over a wide temperature range has been the holy trinity for researchers involved in the structural metallic materials [1]. Alloy design is central to address this issue as it enables us to invoke different strengthening mechanisms and microstructural engineering approaches to achieve this goal. In the last decade, a new class of metallic materials, popularly known as high entropy alloys(HEAs) or multi-component multi-principal element alloys (MPEAs) [1-3] have attracted significant attention due to their vast compositional space in contrast to conventional alloys. HEAs possess remarkable properties; including excellent elevated-temperature strength [4], exceptional fracture toughness at cryogenic temperatures [5], good thermal stability [6, 7], as well as resistance to wear, corrosion and oxidation [8-10], indicating potentially structural and functional applications. These promising properties are mainly attributed to its four core effects, namely high-entropy effects, sluggish diffusion, severe lattice distortion, and cocktail effects [11-14]. However, these new and broad class [15] of material with a spectrum of mechanical properties are very attractive for structural application, the physics of strengthening mechanism in HEAs is still unknown and need to be explored [14, 16-18].In the conventional solid solution alloy systems, the solute atoms primarily contribute to the strengthening. The strengthening is attributed to the resistance offered by randomly distributed solute atoms to the dislocation movement in the solvent lattice. The mismatch of atomic size and elastic modulus between the solvent matrix and solute atom leads to an elastic stress field around the solute atom that has to be overcome by a dislocation to move through the host matrix. Therefore, the force required to overcome a dislocation in the presence of solute is higher than that of 100% solvent matrix. This contributes to solid solution strengthening in dilute substitutional solid solution alloys [19-21]. Solid solution strengthening

models for conventional alloys are well studied and it is agreed that the contribution of solid solution strengthening increases with concentration as well as with increase in atomic size and elastic modulus mismatch between the solute and solvent atoms [20, 22].Similarly, a strong temperature and strain rate dependence of solid solution strengthening in solid solution alloys is well established. The Fleischer model [22] for dilute solid solutions assumes a single non-interactive atom in which each solute atom can act as an isolated pinning site, interacting with a dislocation independently leading to an exponent of 0.5 with composition for solid solution strengthening. In contrast, Labusch model [20]; applied for concentrated alloys considers the collective action of the randomly distributed solute atoms on the glide plane with dislocations, leading to a composition exponent of 0.67 for solid solution strengthening. However, the conventional concept of solid solution strengthening models may not be applicable for HEAs where there is no well-defined solvent and solute. The matrix in HEAs is considered to a whole-solute matrix with no well-defined solute. To overcome this issue, recently, Toda-Caraballo *et.al*. [23, 24] and Varvenne *et al*.[25,26] formulated solid solution models, which are an extension of Labusch model [20].According to the model proposed by Toda-Caraballo, the average inter-atomic distance depends upon solute concentration in an alloy and the solid solution strengthening is related to the binary solute-solvent interactions in a HEA. In contrast, Varvenne and co-workers predicted the yield strength of FCC HEAs and its equiatomic subset, which is quantitatively successful. It describes that each solute atom is embedded in a reference 'defective matrix' carrying average properties of the alloy and thus neglect the concept of solvent and solute. The model selects solute misfit volume as the main factor for the strengthening. This, in turn, leads to severe lattice distortion in the whole solute matrix making strain field around the bigger atom non-uniform and adding to the solid solution hardening. A recent experimental

investigation [27] shows that doping of the Cantor alloy by vanadium having a large misfit volume compared to other elements, leads to significant improvement in strength. Similarly, Yin *et al*.[28] showed that the addition of Pd in quaternary CoCrFeNi alloy led to significant improvement (250%) in yield strength. This enhanced strength is primarily attributed to large misfit volume induced by Pd. Despite the few scattered studies in the literature, a systematic investigation to address the challenging problem of the effect of misfit volume of the solute atoms on solid solution strengthening in HEAs is not available. However, it is evident that such research is widely needed to understand the solid solution hardening in HEAs.

In this background, the present work reports the effect of systematic addition of Al to equiatomic CoCrFeMnNi in varying concentration (0.25-5atom %) to investigate the strength of the Cantor alloy. This alloy exhibits relatively low yield and ultimate tensile strength. This is mainly attributed to the fact that the Cantor alloy has single phase microstructure and the insufficient amount of lattice distortion [29], responsible for solid solution strengthening. Since the atomic radius of the element in Cantor alloy are almost similar (r_{Fe} = 0.126, r_{Cr} = 0.128, r_{Mn} = 0.127 and r_{Ni} = 0.125 nm). Therefore, the addition of Al (r_{Al} = 0.143 nm) is likely to induce a sufficient amount of lattice distortion, causing the pronounced effect on solid solution strengthening in the Cantor alloy.Al is added in varying concentration (up to 5atom%) to preserve the FCC structure. Beyond 5 atomic % Al, secondary BCC/B2 phase was observed along with primarily FCC phase[30]. By using state of the art materials processing, testing and characterization tools, varioussolid solution hardening models have been employed to explain the observed results and predict the evolution of yield strength with aluminium addition in the concentrated Cantor alloy.

2. Materials and Methods

Prior to the description of the experimental result in the present investigation, it is important to briefly describe the available solid solution strengthening models for the conventional alloys as well as multi-component multi-principal alloy system.

2.1 Solid Solution Strengthening Theory

Lattice distortion has a pronounced effect on solid solution strengthening of an alloy by introducing the barrier to the dislocation motion. The strengthening mechanism in thealloys was first introduced by Fleischer who assumed that motion of dislocations pinned by an isolated solute atom and thus only applicable for dilute solute content. Following this assumption, he came up with an expression for solid solution hardening:

$$\Delta\sigma_{ss} = B_i X_i^{1/2} \qquad (1)$$

Here B_i is hardening parameter which is a function of lattice mismatch($\frac{da}{dX_i a}$) and modulus mismatch,($\frac{d\mu}{dX_i \mu}$). X_i is the solute content. Labusch considered the frictional effect due to continuous interaction of an edge dislocation with a group of solute atoms rather than pinning of dislocation by an isolated solute atom to explain solid solution strengthening in conventional solid solutions. Based on this approach, he concluded the expression similar to that of Fleischer model; with a different exponent to X_i

$$\Delta\sigma_{ss} = B_i X_i^{2/3} \qquad (2)$$

Both models are very similar in terms of modulus, and lattice mismatch and the experimental investigations show good agreement of $\Delta\sigma_{ss}$ obtained from the experiment fitted against $X_i^{1/2}$ [31, 32] and $X_i^{2/3}$ [32]. Nonetheless, most of the literature data show better agreement with

Labusch model. Hence, taking into this consideration, Toda-Caraballo *et al.*[23]and Varvenne *et al*. have recently extended this approach to HEAs. Toda-Caraballo *et al.*[23]have formulated a new method for modelling solid solution strengthening in HEAs, which employs the fact that inter-atomic distance(s) in the alloy is affected by the solute atoms. In this method, the inter-atomic spacing of a binary alloy can be calculated using the lattice parameter; average inter-atomic spacing (s^{avg}) varies with the mole fraction of species in the alloy and approximated by:

$$s^{avg} = (X_1 \cdots \cdots X_n)\begin{pmatrix} s_{11} & \cdots & s_{1n} \\ \vdots & \ddots & \vdots \\ s_{n1} & \cdots & s_{nn} \end{pmatrix}\begin{pmatrix} X_1 \\ \vdots \\ X_n \end{pmatrix} \qquad (3)$$

Using this approach $\frac{ds}{dX_i}$ (equivalent to $\frac{da}{dX_i}$) was calculated, which is subsequently used to calculate the hardening parameter $B_i$and thus $\Delta\sigma_{ss}$. A detailed formulation of this approach is provided in Ref [15].

Vereven *et al*. developed a generalized model for solution strengthening of any FCC alloyof different compositions, including HEAs, which is found to be effective in predicting the yield strength of the CoCrFeMnNi equiatomic HEA and its equiatomic subsets. It describes each element in an alloy as a "solute" embedded into an effective "solvent", carrying all the average properties of the alloy, *i.e.,* the model considers the substitutional atoms causing a local fluctuation in composition with respect to an effective-medium considered as 'reference defective' matrix which is shown in Figure 1.So, the strengthening arises due to interaction between dislocations and any local fluctuation in an effective medium such that dislocation adopts a wavy appearance to move in minimum energy configuration region but at the expense of an increase in dislocation line length. Accordingly, yield strength is provided by:

$$\tau_{y0} = 0.01785\left[\frac{\Gamma}{b^2}\right]^{-1/3}\left[\mu_{alloy}\frac{1+\nu_{alloy}}{1-\nu_{alloy}}\right]^{4/3} \times \left[\frac{\sum_n c_n \Delta V_n^2}{b^6}\right]^{2/3} \qquad (4)$$

$$\Delta E_b = 1.5618\left[\frac{\Gamma}{b^2}\right]^{1/3} b^3 \left[\mu_{alloy}\frac{1+\nu_{alloy}}{1-\nu_{alloy}}\right]^{2/3} \times \left[\frac{\sum_n c_n \Delta V_n^2}{b^6}\right]^{1/3} \quad (5)$$

The predicted tensile yield stress is

$$\sigma_y(T,\varepsilon) = 3.06\tau_{y0}\left[1-\left(\frac{kT}{\Delta E_b} ln\frac{\dot{\varepsilon_0}}{\dot{\varepsilon}}\right)^{2/3}\right] \quad (6)$$

Here, τ_{y0} zero-temperature shear yield stress, ΔE_b = Energy barrier (associated with dislocation segment of length ζc), ΔV_n = The solute misfit volumes, Γ =αμb^2, Edge dislocation line tension, μ = shear modulus, ν =Possion's ratio.

Here $\dot{\varepsilon_0}$=10^{-4} is a reference strain, and the prefix 3.06 corresponds to the Taylor factor for isotropic polycrystalline material without any textural effect. The above calculation is based on the edge dislocation without consideration of stacking fault width (d > 6b) [28]. Thus, application of this model requires only solute misfit volume, elastic constant and lattice constant. The reduced and full detailed of this theory are available elsewhere [25, 26, 33].

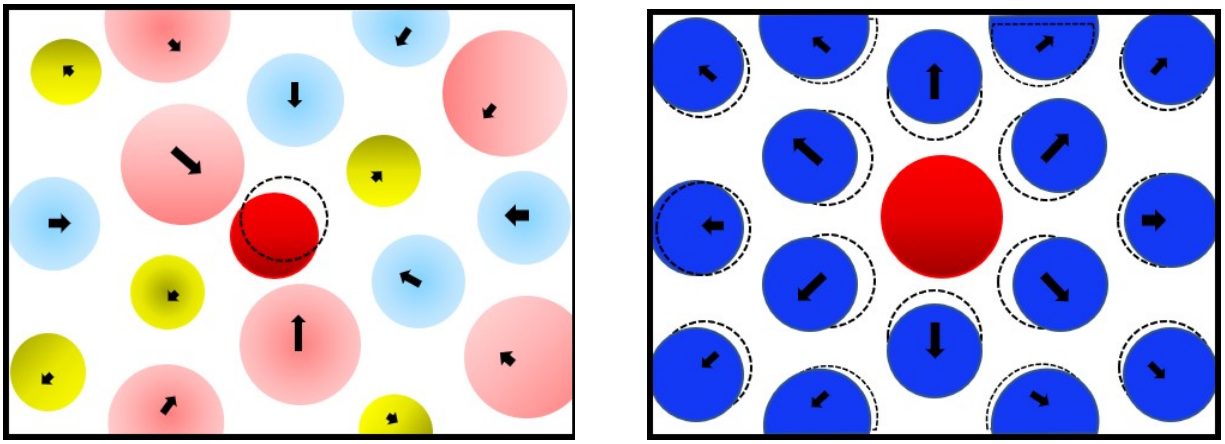

Figure 1: (a) Represents true HEA while (b) represents solute embedded in effective medium

2.2 Alloy preparation and characterization

Bulk $(CrCoFeMnNi)_{100-x}Al_x$ HEAs sample (abbreviated as CAl_x where x = 0, 0.5,1,1.25, 2, 3, 4, 5, atom %),were fabricated using high purity Fe,Co,Cr,Mn,Ni and Al (>99.9%) using vacuum arc melting furnace. The furnace was filled with high purity argon gas prior to melting on a water-cooled copper hearth with a non-consumable tungsten electrode. A Ti gettered sample was melted prior to the melting the elements. The alloys compositions were melted in a pre-evacuated chamber backfilled with high purity Ar gas at current 1200 mA. The pellets were flipped and re-melted at least five times to ensure chemical homogeneity. They were suction cast to produce a billet of 60 mm × 10mm × 10 mm in a water-cooled copper mould in an Ar containing vacuum chamber post evacuated at 10^{-7} millibar pressure. Subsequently, the billets were sealed in a quartz tube filled with argon gas and homogenized at 1273 K for 24 h, followed by quenching in water. The compositional homogeneity of the homogenized samples (1273K/24h.) was probed near atomic resolution using local electrode atom probe tomography (LEAP 5000 XR) [34]. The APT samples were prepared using focused ion beam (FIB).The homogenized samples were polished using emery papers (P1000, P1500, P2000 and P2500) followed by cloth polishing in alumina suspension (1μm). The final stage of polishing was carried out in a vibromet (Vibromet, Buehler, U.S.A.) machine using colloidal silica suspension (particle size = 0.05) prior to APT tips preparation.

Each of these billets was cold rolled to 50% rolling reduction and followed by recrystallization at 1273K for two hours in quartz sealed tube in the presence of Ar atmosphere to obtain a fully recrystallized microstructure and eliminate the casting defects. The rolled samples were machined out using high precision wire electric discharge machining (EDM) to prepare ASTM E8 standard flat dog-bone shaped mini tensile specimens (7 mm gauge length, 3 mm width and

1mm thickness) with the rolling direction parallel to the tensile direction to avoid any strength contribution from the rolling texture. The uniaxial tensile tests were carried out on 100 kN Instron-1195 universal testing machine to determine yield strength (YS), ultimate tensile strength (UTS) and % elongation. The tensile tests were carried out at a crosshead velocity of 0.42 mm/min corresponding to a strain rate of 0.001 $s^{-1}$with tensile axis parallel to the prior rolling direction. The tests were performed at least three times for each alloy composition to obtain statistically significant data. Hardness measurements were also performed using Vicker micro-hardness with a diamond pyramidal indenter and 1Kg force as well as dwell time of 10 seconds. Average hardness value was obtained from ten reading for each alloy composition.

The crystal structure of the homogenized (1273K/24h.) samples were determined using X-ray diffraction (Cu-K_α radiation (λ = 0.15402 nm) Empyrean Panalytical diffractometer) with a step size of 0.02, at voltage 45 kV and 40 mA current. $K_{\alpha 2}$stripping and background noise subtraction were carried out using X'Pert high score plus software. The lattice parameter of different phases was calculated using Rietveld refinement of the XRD patterns.The detailed microstructural investigation of the homogenized samples was carried out using field emission gun scanning electron microscope (NOVA NANO SEM 450) equipped with an electron back-scattered diffraction (EBSD, FEI, TSL-OIM).Samples preparation for EBSD was carried out using emery paper of grit size P1000,P1200,P1500 and P2000, subsequently followed by cloth polishing in alumina suspension of particle size 1μm. The final stage of polishing was performed in vibromet (Vibromet, Buehler, U.S.A.) machine using colloidal silica suspension of dispersed particle size 0.05μm for 12 hours. The fine-scale microstructural characterization of tested tensile samples was carried out using transmission electron microscopy (FEI Tecnai UT20 twin T.E.M with an accelerating voltage of 200 kV) coupled with selected area electron pattern. Specimens were

machined out near the fracture tip in the form of a disc of diameter 3 mm and mechanically grounded to a thickness of 100µm, followed by electro-polishing in a twin-jet polisher using an electrolyte (80% methanol and 20% perchloric acid) cooled by liquid nitrogen temperature.

3. Results

3.1 Microstructures and Phase evolution as a function of Al concentration

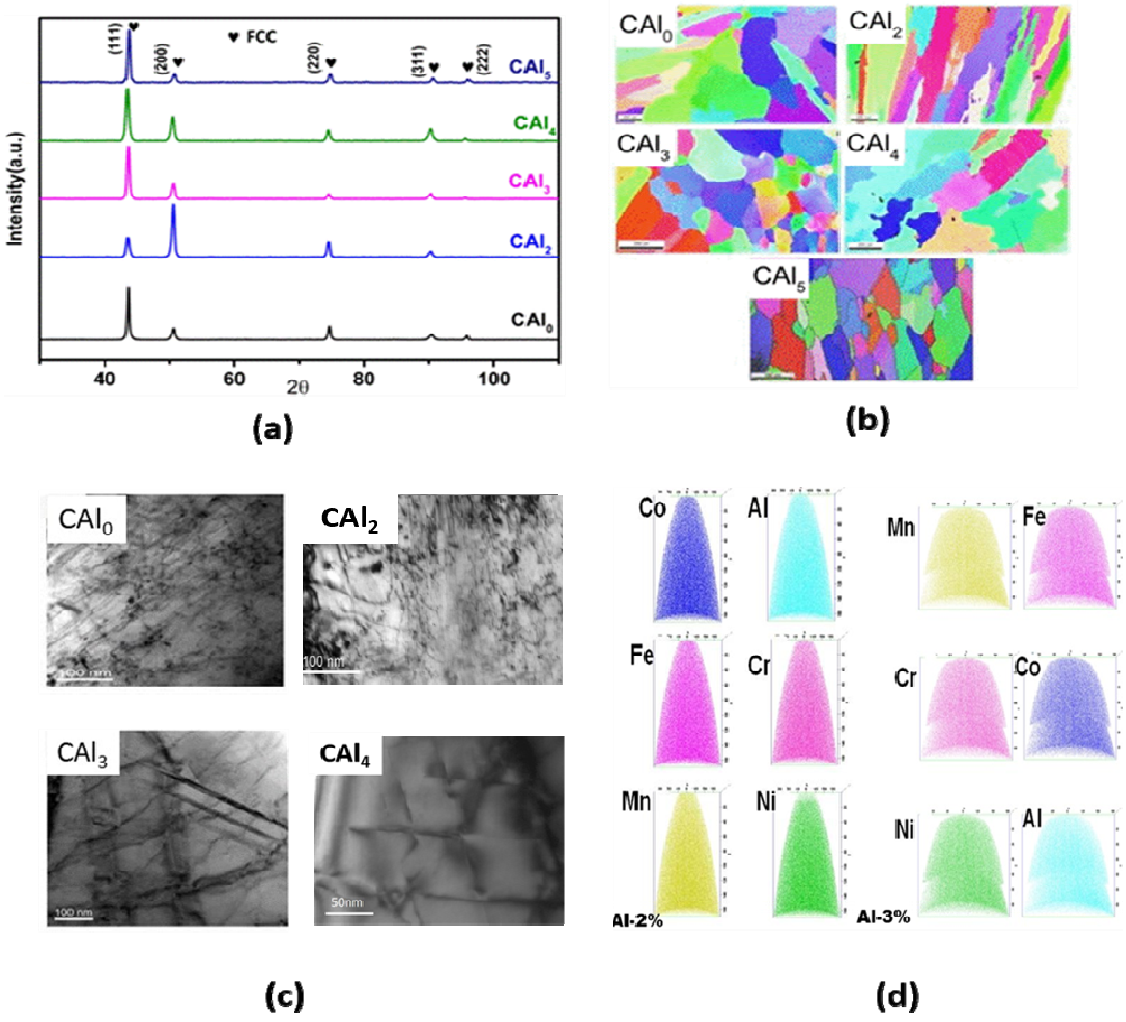

Figure 2: (a).XRD patterns of homogenized samples of CAl_x (Where x=0,2,3,4,5 at.%),(b).Electron Backscattered diffraction micrographs of the homogenized CAl_x, (c).TEM Image of Tensile specimen CAl_0, CAl_2,CAl_3 and CAl_4, (d). APT image of CAl_2 and CAl_3

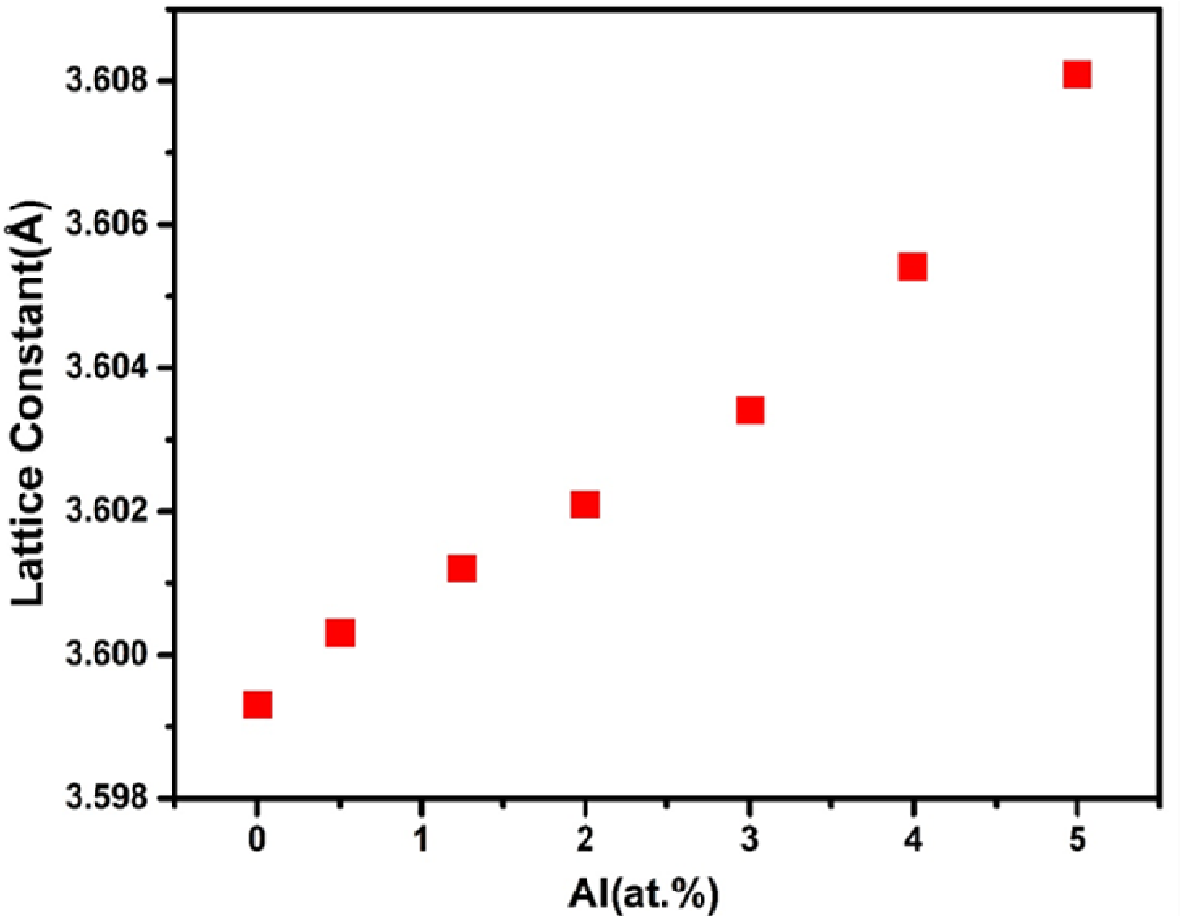

Figure 3: Lattice parameter of the investigated alloys as a function of Al concentration

The X-ray diffraction pattern of the homogenized samples with varying aluminium concentration (Al atomic percent = 0, 0.5, 2, 3, 4, 5) is recorded as shown in Figure 2a. The patterns show the characteristic peak of the FCC phase with a lattice parameter of 0.35993 nm for the Cantor alloy. The Al addition preserves the FCC phase without formation of any unwanted phase. However, the shift in the position peak to lower 2θ value was observed, indicating an increase in the lattice parameter with progressive addition of Al. This leads to lattice expansion in aluminium containing Cantor alloy. The lattice parameter of FCC phase in all alloys has been determined

using the Rietveld Method, shown in Figure 3. There is a significant increase in the lattice parameter on the continuous increase in Al concentration to Cantor alloy.

In order to further study the microstructural evolution caused by the Al addition to the Cantor alloy, SEM-EBSD inverse pole figure map of the homogenized sample with varying Al concentration has been carried out, shown in Figure 2b. All micrographs exhibit with a similar polycrystalline structure without any detection of the second phase, consistent with X-ray diffraction pattern in Figure2a. Importantly, all microstructures show similar grain size (~100 μm) indicating that Al may have negligible effect on the grain size of the alloys.

Figure 2d shows the results of APT investigation of the homogenized samples. Evidently, no elemental segregation of the alloying elements (Co, Cr, Fe, Mn, Ni and Al) was observed indicating random solid solution nature of the given alloys.

3.2 Mechanical Behaviour of Alloys

Let us now discuss the mechanical properties of the alloys. Hardness of the homogenized (1273K/24 h) samples has been recorded and shown in Figure 4 a. Hardness is found to increase monotonically with an increase in Al concentration. Tensile investigation of the homogenized (1273K/24 h) samples has been recorded and shown in Figure 4 a. Hardness is found to increase monotonically with an increase in Al concentration. Tensile test results from the cold rolled and annealed samples with similar grain size also show a similar trend of increase in yield strength and ultimate tensile strength with addition of aluminium. In addition, the tensile test results show

insignificant reduction in ductility with increase in aluminium content. This has been displayed in Figure 4 b. The YS, UTS and elongation to fracture have been reported in Table 1.

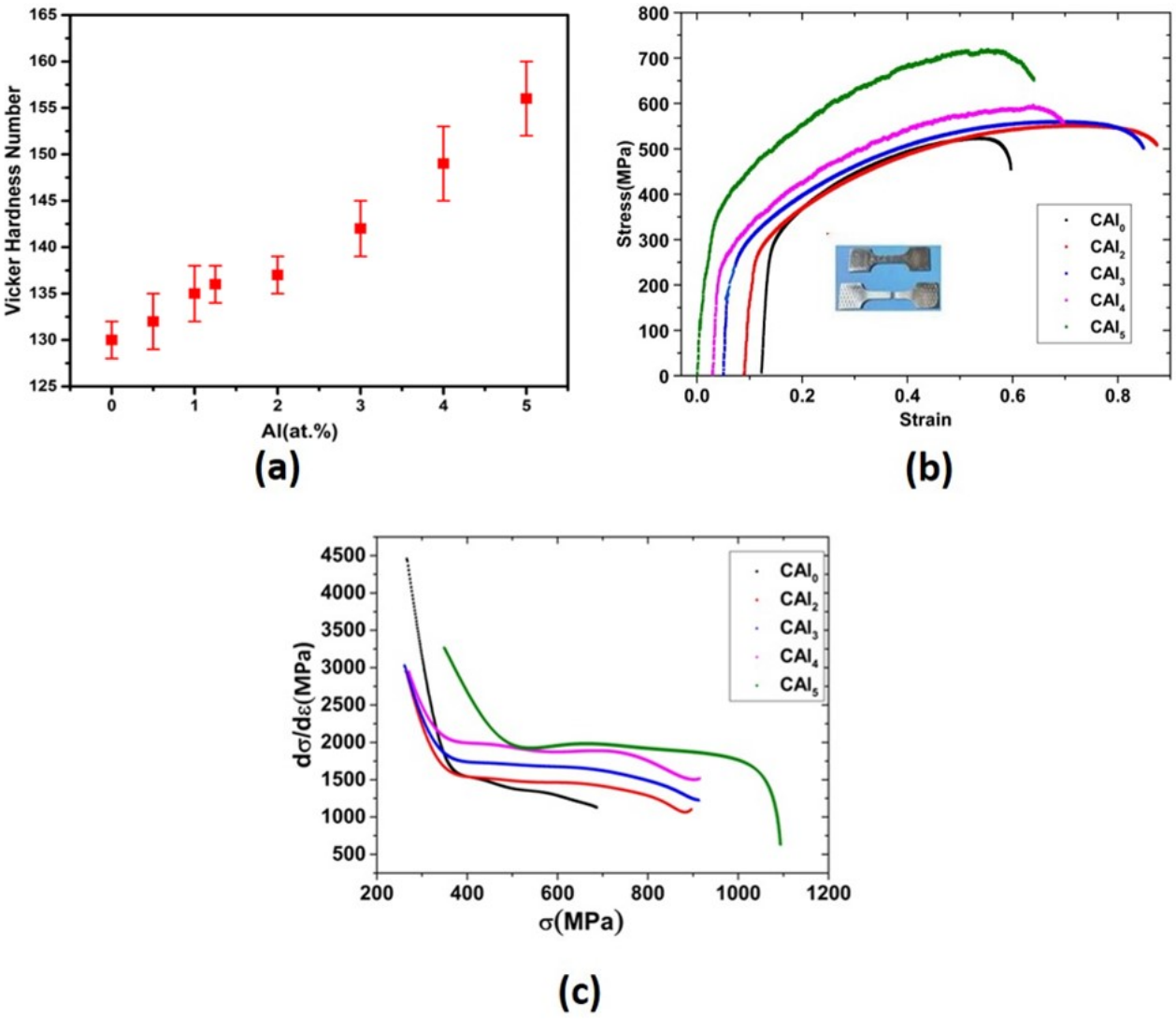

Figure 4: (a).Vicker Hardness Number for CAl_x (Where x= 0,0.5,1,1.25,2,3,4 and 5), (b).Stress- strain curve for CAl_x, (c). Strain-hardening curve forCAl_x (Where x=0,2,3,4,5) .

Table 1: Mechanical Properties of Different Alloys

Composition	Y.S. (MPa)	UTS(MPa)	% elongation	Strain Hardening Exponent
CAl_0	240±8	522±17	64	0.5
CAl_2	253±13	551±48	81	0.44
CAl_3	254±12	560±41	82	0.47
CAl_4	268±15	595±36	69	0.49
CAl_5	321±21	718±39	66	0.48

To further understand the deformation behavior of all the investigated alloys, strain hardening rate ($d\sigma/d\varepsilon$) derived from the true stress-strain curve was plotted against true stress (σ), as shown in Figure 3c. The curves correspond to stage III of the work hardening and hence sensitive to temperature and strain rate. The onset of stage III begins when the flow stress curve deviates from linearity; where cross-slip is considered to be the rate controlling step. The curve corresponds to CAl_0 in Figure 4c, where strain hardening rate decreases continuously with true stress as a result of dynamic recovery. This is generally observed in the alloys with face centered cubic crystal structure[35]. While on the addition of Al, curves for CAl_2, CAl_3, CAl_4 and CAl_5have exhibited with three distinct regions of work hardening rate at room temperature, This behaviour is similar to the Cantor alloy tested at liquid nitrogen temperature[36]. Initially, strain hardening rate decreases with true stress same as to curve CAl_0, followed by almost constant work hardening rate (plateau region).

The fine-scale microstructure characterization and phase evolution of the tensile tested sample near the fracture tip have been carried out using TEM as a function of different Al content to understand the different phases, size, morphology and defect structure. Figure 2c shows the

bright field images of the Cantor alloy with different Al concentration. It has been observed that the Cantor alloy shows single-phase FCC crystal structure with inset showing selected area diffraction pattern (SADP). The alloys containing Al also reveal FCC structure. In addition, the bright field images show defect structure, profuse dislocation activity (Figure 3c).

4. Discussion

All alloys exhibit single-phase FCC homogeneous solid solution which has been verified by XRD, SEM-EBSD inverse pole figure maps (Figure 2b) as well as atom probe tomography (Figure 2c). For the FCC alloys, lattice parameter increases with the gradual increase in Al concentration (Fig1).The investigation of the mechanical behaviour shows that the hardness, YS and UTS increase with progressive addition of Al, indicating a solid solution strengthening effect possibly induced by the enhanced lattice distortion as the atomic radius of Al is larger (approx. 12-13%) than the rest of the elements. The major contribution of the strengthening comes from solid solution strengthening since alloy is single phase with similar grain sizes. The Hall-Petch strengthening and strengthening due to strain hardening have no significant contribution, details of which are provided in the Supplementary Information.

In order to estimate the potency of solid solution strengthening, we have adopted constitutive modeling using four different models to single phase FCC $(CoCrFeMnNi)_{100-x}Al_x$alloys(x=0-5 at.%) in Figure 4. It shows the behaviour corresponding to various models for solid solution hardening to predict the YS of the alloys. There is a large deviation between the predicted and experimental values for the Fleischer and Labusch models. Toda-Caraballo *et al*. [23] also utilized the solid solution strengthening model for the multi-component alloy. Although this model is an extension of Labusch, the main feature of this model is the calculation of the lattice

parameter of the alloy and its variation with composition utilizing the fact that the dependency of inter-atomic distance with solute contents shown in Fig 4a. The YS is shown as a function of Al concentration is predicted by Toda-Caraballo *et al*. [23]. There is no reasonable agreement between the predicted one with the experimental results.

Varvenne *et al*. [25,26] predicted the solid solution strengthening of multi-component alloys assuming an approach of equiatomic compositions, single-phase and random solid solution alloys. In this model, the highly concentrated alloys use each component as a solute atom embedded in an effective medium of average composition. Hence, it averages out the effect of all solutes in a multi-component system such as lattice constants, Burgers vectors and elastic properties. We show here that the strengthening cause by Al addition in the Cantor alloy can be explained theoretically by considering the completely random substitutional alloy.

Apparently, there are similarities between models by Toda-Caraballo *et al*. and Varvenne *et al*. Both the models can predict the strengthening in multi-component systems choosing only simple parameters, such as lattice constants and elastic properties. Both models use the concept of the misfit parameter to predict the solute strengthening of a multi-component system. The work described by Toda-Caraballo *et al*. based on the lattice misfit calculation of the element in the alloy to determine solid solution strengthening effect. The lattice parameters of all constituent in Cantor alloys do not vary much, so misfit calculations associated with it is not expected to differ much. It is generally considered that HEAs have a severely distorted lattice, but local lattice distortion in the Cantor alloy measured by neutron scattering is reported to be moderate[37]. However, the addition of Al to the Cantor alloy, which has a larger lattice parameter than the rest of the elements, can induce a significant amount of lattice distortion. The strain field associated

with these distortions impedes the motion of dislocation in the glide plane cause solid solution strengthening.

In contrast, Varvenne *et al*. utilized the concept of the average volume misfit to evaluate the effect of the solid solution strengthening in the multi-component alloy, which shows good agreement with the experimental value in this present work as shown in Fig. 4. The apparent volume for aluminium is larger than the rest of the element, which is given in Table 2, which is used to calculate the misfit volume that further used in the calculation of predicted yield strength of the alloys .Both concepts principally use Labusch's model approach and consider the dependence of shear stress with temperature and composition.

Despite the similarities between both models, the model developed by Varvenne et al. is more efficient to predict the yield strength of the multi-component system in terms of activation energy to move dislocation and temperature dependency of yield stress. This model not only considers the interaction energy of dislocation's stress field with the solute misfit strain but also consider the chemical misfit due to change in the bonding environment of the solute in the partial dislocation core structure and the stacking fault region between the partials. So, this model has a better correlation between the predicted yield stress and the yield stress determined experimentally for temperature range 78 K to above the room temperature[25, 26]. While Toda - Caraballo's model of solid solution hardening to predict the yield strength is independent of temperature. In this model, the atomic size mismatch dominates the yield strength of the alloy because the term 'α' (α = 16 which represent the interactions forces between edge and screw dislocation and the solute atoms) associated with lattice mismatch and neglecting the effect of modulus mismatch in the calculation of the hardening parameter 'B'. However, this model has shown good agreement with the experimental yield stress of the some FCC alloys like

CoCrFeMnNi and its subset where the shear moduli are nearly the same but not the alloys like $AlCoCrFeNiTi_x$ (x= 0.1), CrCuFeMnNi and some more [23, 24]. At the same time, this model also requires appropriate atomic radii [38] in calculating the average interatomic spacing, which is not necessary in case of Varvenne model. Even with the use of proper atomic radii and shear moduli the comparison between predicted yield strength and experimental yield strength is not well [39]. So, in order to improve the Toda-Caraballo model of solid solution hardening, one must incorporate the modulus mismatch in the same manner as the formation of the matrix for calculates the average interatomic spacing to calculate the hardening parameter which is shown by Coury *et al*. [39]. This model does not take into account of the dislocation core structure and variation in the energy barrier concerning compositions and materials quantities. In comparison to the model developed by Toda-Caraballo *et al*. the concept of effective medium matrix incorporates the effect of fluctuation in the stress field due to the presence of solute on dislocation line tension and thus bring the idea about the mesoscopic fluctuation in stress as a result of solution hardening response [40].

Unlike conventional solid solution alloys, HEAs are 100% solvent alloys and hence it is difficult to estimate the contribution from lattice and modulus mismatch as these are locally defined rather than globally defined and fixed for a dilute alloy. It has already been postulated that the dislocation movement in HEAs is characterized by motion of shorter dislocation line length compared to conventional alloys. The local interaction of a segment of dislocation with the local solute atmosphere is therefore, important in determining the solid solution response. This democratization of strengthening due to interaction of smaller dislocation segments with local solute clusters may reduce the potency of solid solution strengthening. This indeed is true as solid solution strengthening in HEAs is not in accordance with the conventional solid solution

strengthening models, but the positive effect is that there is no drastic decrease in ductility as observed for conventional solid solution alloys due to exhaustion of mobile dislocations with deformation. It is no surprise that Cantor alloy with constituent elements that have similar atomic sizes and similar modulus shows modest solid solution strengthening but excellent ductility. Even on addition of Al, there is increase in strength but without significant loss in ductility. This can be explained on the basis of smaller dislocation segments participating in the local pinning events in a 100% solvent alloy compared to a dilute alloy wherein large dislocation segments are pinned by solutes. The pinning of smaller dislocation segments makes availability of mobile dislocations that contributes to little loss in ductility. Al has a significantly lower elastic modulus than other elements of the Cantor alloy but a significantly larger size and it is expected that the distortion caused in the lattice due to presence of Al atom will lead to an interaction between the stress field of an edge dislocation and the stress field of the aluminium atom contributing to strengthening. It is, therefore, logical that the Varvene's model that considers strengthening due to atomic volume shows better match for Cantor alloy with aluminium addition.

Table 2: Apparent volume of different elements and alloy

Element	Apparent volume $(Å)^3$
Fe	12.09[a]
Co	11.12 [a]
Cr	12.27 [a]
Mn	12.60 [a]
Ni	10.94 [a]
Al	15.74 to 15.77 [b]
FeCoCrMnNi	11.67[c]

[a]Varvenne et.al.[25-26], [b]Rule of Mixture, [c]Basu et.al. [40]

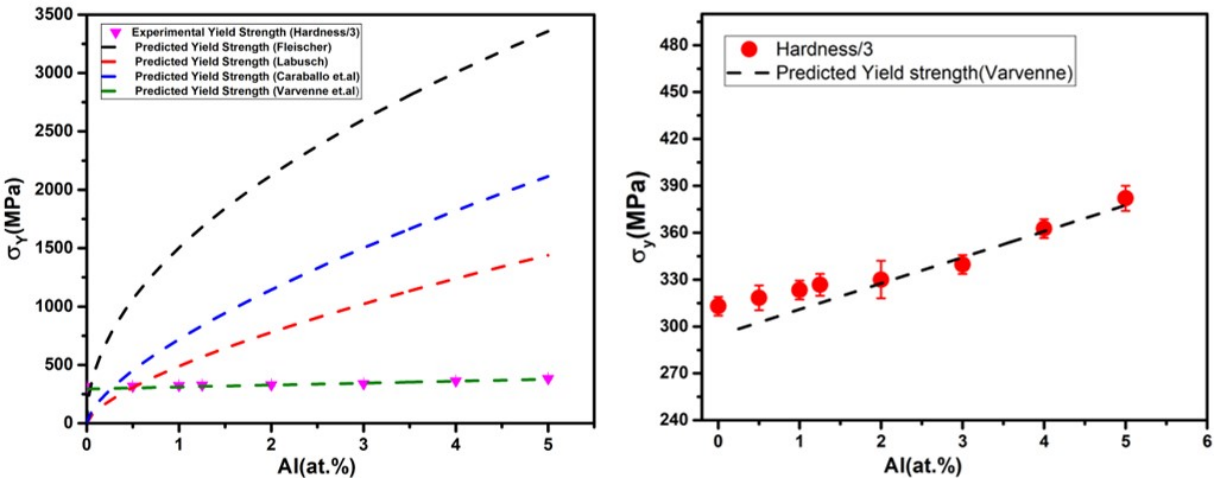

Figure 4.Predicted yield strength with varying Al concentration along with experimental yield strength value for different solid solution hardening model.

5. Conclusions

The microstructural and mechanical properties of a series of alloy $(CrCoFeMnNi)_{100-x}Al_x$ (x=0.25 to atom%) has been characterized and evaluated in the present investigation. Effect of Al addition on phase evolution, hardness, strength and ductility had been discussed. Based on these results and analyze, the following conclusions can be obtained.

(a) The addition of Al to Cantor alloy in the composition range of 0.25 to 5 percent leads to formation of single-phase FCC structure with similar grain size (~100μm) characterized by a continuous increase in hardness with increase in aluminium content.

(b)There is an increase in yield strength and ultimate tensile strength with little loss in ductility with increase in aluminium content. Detailed microstructural characterization indicates slip dominated deformation in all the investigated alloys.

(c) All alloys mainly behave like a solid solution alloy with Al atom acting as a primary source of strengthening as Al has large apparent volume (0.015 $Å^3$) with respect to the rest of the element cause large misfit volume.

(d) The unique not so strong but effective solid solution strengthening observed in Al containing Cantor alloy as explained by the atomic misfit volume can be credited with little loss in ductility with increase in strength by solid solution strengthening.

References

[1] D.B. Miracle, O.N.J.A.M. Senkov, A critical review of high entropy alloys and related concepts, 122 (2017) 448-511.

[2] M. Tasi, J.-W.J.M.R.L. Yeh, High-entropy alloys: Acritical review, 2(3) (2014) 107-123.

[3] D.J.N.c. Miracle, High entropy alloys as a bold step forward in alloy development, 10(1) (2019) 1-3.

[4] C. Tong, M.-R. Chen, S.-K. Chen, J. Yeh, T. Shun, S. Lin, S.J.M.M.T.A. Chang, Mechanical performance of nanostructured CuCoNiCrAlxFe high-entropy alloy system with multi-principal elements, 36 (2005) 1263-1271.

[5] B. Gludovatz, A. Hohenwarter, D. Catoor, E.H. Chang, E.P. George, R.O.J.S. Ritchie, A fracture-resistant high-entropy alloy for cryogenic applications, 345(6201) (2014) 1153-1158.

[6] V. Dolique, A.-L. Thomann, P. Brault, Y. Tessier, P.J.S. Gillon, C. Technology, Thermal stability of AlCoCrCuFeNi high entropy alloy thin films studied by in-situ XRD analysis, 204(12-13) (2010) 1989-1992.

[7] M.-H. Tsai, C.-W. Wang, C.-W. Tsai, W.-J. Shen, J.-W. Yeh, J.-Y. Gan, W.-W.J.J.o.t.E.S. Wu, Thermal stability and performance of NbSiTaTiZr high-entropy alloy barrier for copper metallization, 158(11) (2011) H1161.

[8] Y. Chou, Y. Wang, J. Yeh, H.J.C.S. Shih, Pitting corrosion of the high-entropy alloy Co1. 5CrFeNi1. 5Ti0. 5Mo0. 1 in chloride-containing sulphate solutions, 52(10) (2010) 3481-3491.

[9] Y.-F. Kao, T.-D. Lee, S.-K. Chen, Y.-S.J.C.S. Chang, Electrochemical passive properties of AlxCoCrFeNi (x= 0, 0.25, 0.50, 1.00) alloys in sulfuric acids, 52(3) (2010) 1026-1034.

[10] M.-H. Chuang, M.-H. Tsai, W.-R. Wang, S.-J. Lin, J.-W.J.A.M. Yeh, Microstructure and wear behavior of AlxCo1. 5CrFeNi1. 5Tiy high-entropy alloys, 59(16) (2011) 6308-6317.

[11] B. Cantor, I. Chang, P. Knight, A.J.M.S. Vincent, E. A, Microstructural development in equiatomic multicomponent alloys, 375 (2004) 213-218.

[12] J.W. Yeh, S.K. Chen, S.J. Lin, J.Y. Gan, T.S. Chin, T.T. Shun, C.H. Tsau, S.Y.J.A.E.M. Chang, Nanostructured high-entropy alloys with multiple principal elements: novel alloy design concepts and outcomes, 6(5) (2004) 299-303.

[13] W.-H. Wu, C.-C. Yang, L. Yeh, Industrial development of high-entropy alloys, Annales de Chimie-Science des materiaux, Paris; New York: Masson, 1978-, 2006, p. 737.

[14] Y. Zhang, T.T. Zuo, Z. Tang, M.C. Gao, K.A. Dahmen, P.K. Liaw, Z.P.J.P.i.M.S. Lu, Microstructures and properties of high-entropy alloys, 61 (2014) 1-93.
[15] M.G. Poletti, L.J.A.M. Battezzati, Electronic and thermodynamic criteria for the occurrence of high entropy alloys in metallic systems, 75 (2014) 297-306.
[16] D.B. Miracle, J.D. Miller, O.N. Senkov, C. Woodward, M.D. Uchic, J.J.E. Tiley, Exploration and development of high entropy alloys for structural applications, 16(1) (2014) 494-525.
[17] Z. Wu, H. Bei, F. Otto, G.M. Pharr, E.P.J.I. George, Recovery, recrystallization, grain growth and phase stability of a family of FCC-structured multi-component equiatomic solid solution alloys, 46 (2014) 131-140.
[18] Z. Wu, H. Bei, G.M. Pharr, E.P.J.A.M. George, Temperature dependence of the mechanical properties of equiatomic solid solution alloys with face-centered cubic crystal structures, 81 (2014) 428-441.
[19] F.J.P.o.t.P.S. Nabarro, Dislocations in a simple cubic lattice, 59(2) (1947) 256.
[20] R.J.p.s.s. Labusch, A statistical theory of solid solution hardening, 41(2) (1970) 659-669.
[21] F.J.P.m. Nabarro, The theory of solution hardening, 35(3) (1977) 613-622.
[22] R.L.J.A.m. Fleischer, Substitutional solution hardening, 11(3) (1963) 203-209.
[23] I. Toda-Caraballo, P.E.J.A.M. Rivera-Díaz-del-Castillo, Modelling solid solution hardening in high entropy alloys, 85 (2015) 14-23.
[24] I.J.S.M. Toda-Caraballo, A general formulation for solid solution hardening effect in multicomponent alloys, 127 (2017) 113-117.
[25] C. Varvenne, A. Luque, W.A.J.A.M. Curtin, Theory of strengthening in fcc high entropy alloys, 118 (2016) 164-176.
[26] C. Varvenne, G.P.M. Leyson, M. Ghazisaeidi, W.A.J.A.M. Curtin, Solute strengthening in random alloys, 124 (2017) 660-683.
[27] B. Yin, F. Maresca, W.J.A.M. Curtin, Vanadium is an optimal element for strengthening in both fcc and bcc high-entropy alloys, 188 (2020) 486-491.
[28] B. Yin, W.J.M.R.L. Curtin, Origin of high strength in the CoCrFeNiPd high-entropy alloy, 8(6) (2020) 209-215.
[29] Y. Zhao, T.J.I. Nieh, Correlation between lattice distortion and friction stress in Ni-based equiatomic alloys, 86 (2017) 45-50.

[30] J. Kumar, N. Kumar, S. Das, N. Gurao, K.J.T.o.t.I.I.o.M. Biswas, Effect of Al addition on the microstructural evolution of equiatomic CoCrFeMnNi alloy, 71(11) (2018) 2749-2758.
[31] A. Akhtar, E.J.P.M. Teghtsoonian, Substitutional solution hardening of magnesium single crystals, 25(4) (1972) 897-916.
[32] C. Cáceres, D.J.J.o.L.M. Rovera, Solid solution strengthening in concentrated Mg–Al alloys, 1(3) (2001) 151-156.
[33] C. Varvenne, W.A.J.S.M. Curtin, Predicting yield strengths of noble metal high entropy alloys, 142 (2018) 92-95.
[34] F. Otto, A. Dlouhý, K.G. Pradeep, M. Kuběnová, D. Raabe, G. Eggeler, E.P.J.A.M. George, Decomposition of the single-phase high-entropy alloy CrMnFeCoNi after prolonged anneals at intermediate temperatures, 112 (2016) 40-52.
[35] E.J.P.i.m.s. Nes, Modelling of work hardening and stress saturation in FCC metals, 41(3) (1997) 129-193.
[36] G. Laplanche, A. Kostka, O. Horst, G. Eggeler, E.J.A.M. George, Microstructure evolution and critical stress for twinning in the CrMnFeCoNi high-entropy alloy, 118 (2016) 152-163.
[37] L. Owen, E. Pickering, H. Playford, H. Stone, M. Tucker, N.J.A.M. Jones, An assessment of the lattice strain in the CrMnFeCoNi high-entropy alloy, 122 (2017) 11-18.
[38] F.G. Coury, K.D. Clarke, C.S. Kiminami, M.J. Kaufman, A.J.J.S.r. Clarke, High throughput discovery and design of strong multicomponent metallic solid solutions, 8(1) (2018) 1-10.
[39] F.G. Coury, M. Kaufman, A.J.J.A.M. Clarke, Solid-solution strengthening in refractory high entropy alloys, 175 (2019) 66-81.
[40] I. Basu, J.T.M.J.S.M. De Hosson, Strengthening mechanisms in high entropy alloys: Fundamental issues, 187 (2020) 148-156.

Supplementary Information

The Effect of Aluminium Addition on Solid Solution Strengthening in CoCrFeMnNi: Experiment and Modelling

Jitesh Kumar, N P Gurao and Krishanu Biswas

Table 1: Calculated Parameter from EBSD data for different alloy composition

Composition	Grain size(μm)	GBCD (Number Fraction)		
		LAGB	CSL	HAGB
CAl_0	105±50	0.66	0.08	0.25
CAl_2	99±47	0.64	0.06	0.29
CAl_3	98±45	0.67	0.08	0.24
CAl_4	103±35	0.74	0.07	0.18
CAl_5	100±40	0.69	0.09	0.21

LAGB: Low angle grain boundary, HAGB: High angle grain boundary, CSL: Coincidence site lattice

Table 2: Various strengthening mechanism along with the parameters contributing in strengthening mechanism

Mechanism	Formula	Parameters	CAl_0	CAl_2	CAl_3	CAl_4	CAl_5
Strain Hardening	$\sigma_{SH} = M * \alpha * G * b * \sqrt{\rho}$ M=Taylor Factor α = Correction factor G = Shear modulus b = Burger vector ρ = Dislocation density	M	3.06	3.06	3.06	3.06	3.06
		α	0.4	0.4	0.4	0.4	0.4
		$G(MPa)$	85000	83820	83230	82640	82050
		$b(nm)$	0.25448	0.25470	0.25479	0.25494	0.25513
		$\rho(m^{-2})$	$3*10^{12}$	$3*10^{12}$	$3*10^{12}$	$3*10^{12}$	$3*10^{12}$
		$\boldsymbol{\sigma_{SH}}$	**25.95**	**25.61**	**25.44**	**25.28**	**25.12**
Hall Petch Strengthening (sample Homogenize at 1273K/24hrs)	$\sigma_{HP} = k_{HP} * d^{-0.5}$ k_{HP} =Hall Petch coefficient d = average grain size	k_{HP}	0.49	0.49	0.49	0.49	0.49
		d (μm)	105	99	98	103	100
		$\boldsymbol{\sigma_{HP}}$	**47.81**	**49.24**	**49.49**	**48.28**	**49**
Hall Petch Strengthening (sample Homogenize at 1273K/24hrs followed 50% reduction and Heat treatment at 1000K/2hrs)	$\sigma_{HP} = k_{HP} * d^{-0.5}$ k_{HP} =Hall Petch coefficient d = average grain size	k_{HP}	0.49	0.49	0.49	0.49	0.49
		d (μm)	60	70	73	65	68
		$\boldsymbol{\sigma_{HP}}$	**63.25**	**58.56**	**57.35**	**60.77**	**59.42**